PHYSICAL REVIEW A **102**, 032808 (2020)

Vibrational excitation of N_2O by an electron impact and the role of the Renner-Teller effect in the process

Hainan Liu,[1] Samantha Fonseca dos Santos,[2] Chi Hong Yuen,[3] Pietro Cortona,[1]
Mehdi Ayouz,[4,*] and Viatcheslav Kokoouline[3]
[1]*Université Paris-Saclay, CentraleSupélec, CNRS, Laboratoire SPMS, 91190 Gif-sur-Yvette, France*
[2]*Department of Physics, Rollins College, Winter Park, Florida 32789, USA*
[3]*Department of Physics, University of Central Florida, Orlando, Florida 32816, USA*
[4]*Université Paris-Saclay, CentralSupélec, LGPM, 91190 Gif-sur-Yvette, France*

(Received 25 May 2020; accepted 21 August 2020; published 11 September 2020)

Cross sections and rate coefficients for vibrational excitation and de-excitation of the N_2O molecule by a low-energy electron for transitions between the lowest vibrational levels are computed using a first-principles approach. The present theoretical approach employs the normal-mode approximation for the description of target vibrational states, the vibrational frame transformation to compute amplitudes of vibrational transitions, and the *R*-matrix method to compute *ab initio* electronic bound and continuum states. It was found that the nonadiabatic Renner-Teller effect, which couples partial waves of the incident electron with degenerate bending vibrations of N_2O, is responsible for the excitation of the bending mode. Theoretical results obtained agree reasonably well with available experimental data at low energies. Thermally averaged rate coefficients are computed for temperatures in the 10–10 000 K range.

DOI: 10.1103/PhysRevA.102.032808

I. INTRODUCTION

Vibrational (de-)excitation by electron impact is a process in which an electron scatters off a molecule and exchanges energy with it in a way that leaves the molecular target in a different vibrational state. For N_2O, vibrational (de-)excitation can be depicted by

$$e^- + N_2O(\nu_i) \to e^- + N_2O(\nu_i{}'), \qquad (1)$$

where ν_i and and ν_i' denote the initial and final vibrational states of N_2O, respectively.

Due to the importance of nitrous oxide (N_2O) in a plethora of research fields ranging from astrochemistry [1–3] to low-temperature plasma technology [4] and medicine [5], different electron-N_2O collisional processes have been experimentally and theoretically explored over the years. Differential and integrated cross sections for elastic and certain inelastic processes have been measured by several groups [6–26]. Although the experimental investigations generally agree on the position of an observed resonance near 2.3–2.5 eV, they disagree on the assignment for the symmetry of the resonant state. Furthermore, there is also disagreement with respect to a second resonance observed around or above 8.0 eV. On the theoretical side, the earlier studies by Morgan [27], Sarpal *et al.* [28], and Bettega *et al.* [29] aimed at clearly specifying the nature of the two resonances observed in the experiments. Morgan and Sarpal *et al.* employed the *R*-matrix method with different models to study electron scattering by N_2O in its equilibrium geometry. They obtained a resonance near 2.3 eV with $^2\Pi$ symmetry. Later, using a slight modification of the Schwinger multichannel method of incorporating polarization effects, Bettega [29] was able to reproduce the experimental features between the two resonances.

To our knowledge, no theoretical vibrational cross sections have been reported to date, while several experimental cross sections have: by Hayashi and Akashi [30], Kitajima *et al.* [18], Allan and Skalický [21], and Nakamura [22]. A compilation of their work can be found in a recent review [31]. Hayashi and Akashi presented cross sections for electron-induced vibrational excitations from electron swarm parameters in pure N_2O. Kitajima *et al.* as well as Allan and Skalický measured absolute differential cross sections for vibrationally inelastic electron scattering with a range of electron scattering energies from the threshold region up to 20 eV. Allan and Skalický reported measurements for only one scattering angle, 135°, and multiplied each of the measured differential cross sections by the factor 4π to estimate the integral cross section. Nakamura [22] derived cross sections for vibrational excitation from swarm parameters.

The present work represents the first theoretical vibrational excitation (VE) study of N_2O by electron impact. We present cross sections and rate coefficients for transitions between ground and first vibrational states of N_2O using the theoretical and computational formalism recently employed to study the VE of NO_2 [32]. The rotational structure is neglected in the present study.

The paper is organized as follows. The next section, Sec. II, describes the theoretical approach and computational details employed in our calculations. In Sec. III, the results obtained numerically are analyzed using the model of Renner-Teller coupling for linear molecules. In Sec. IV, the obtained VE

---

[*] mehdi.ayouz@ecp.fr

cross sections and corresponding rate coefficients are shown and discussed. Section V presents uncertainty estimations of the present approach, and the last section, Sec. VI, is devoted to our conclusions.

II. THEORETICAL APPROACH

Our approach can be summarized as follows. We start by characterizing the molecular target according to its equilibrium geometry, vibrational frequencies, and dipole moment value at equilibrium: features that can be obtained by performing *ab initio* electronic bound molecular states calculations. We proceed by performing *ab initio* electronic continuum molecular states calculations to obtain a scattering matrix at different molecular geometries along the vibrational normal-mode coordinates. We then transform the scattering matrix into the basis of vibrational states of the target molecule. Finally, we compute the vibrational (de-)excitation cross sections from the transformed scattering matrix.

The approach used in our study has been previously described and applied to the NO_2 molecule [32], and a more detailed narrative of the simplified model on which our approach is based can be found in Refs. [33,34]. Therefore, we limit the description presented in this section to the main ingredients of the theoretical formalism—the normal-mode approximation and the vibrational frame transformation—and to the computational details of our calculations.

At low energies around the equilibrium position, the potential energy curve of the most rigid molecules is fairly well described by the quadratic potential of a harmonic oscillator. In our approach, we describe vibrational wave functions of the molecular target using the normal-mode approximation. The approximation allows us to perform a significant part of the calculations analytically. For molecules of astrophysical and low-temperature plasma interest, like N_2O, only the lowest vibrational levels are significantly populated at low temperatures and the range of scattering energies needed to study vibrational excitation is within the validity of the normal-mode model.

After computing the scattering matrix, we perform a vibrational frame transformation [35] to change the scattering matrix obtained for clumped nuclei for a number of molecular geometries to the vibrating-molecule picture that the electron sees when it is at large electronic distances.

The clumped nuclei basis of asymptotic channels is denoted by the channel quantum numbers $\{l, \lambda\}$ that label the angular momentum of the incoming and outgoing electrons and their respective projections on the z axis in the molecular frame coordinate system. The three axes of the molecular coordinate system are chosen along the principal axes on the inertia of the molecule, such that the quantization axis (the z axis) is directed along the molecular axis in calculations for linear geometries. For bent geometries of the molecule, the z axis is perpendicular to the plane of the molecule, with the x axis aligned along the axis of the smallest moment of inertia. In Sec. III we introduce another set of quantum numbers $\{l, \tilde{\lambda}\}$ and corresponding channel functions, which replace the spherical harmonic Y_l^λ with their real-valued combinations of $Y_l^{\pm\lambda}$. The target vibrational wave functions are labeled by the $\{\nu_i, \nu_i'\}$ set of quantum numbers.

The vibrational frame transformation of the scattering matrix elements is given by

$$S^{\nu_i'\nu_i}_{l'\lambda',l\lambda} = \langle \chi_{\nu_i'}(\mathbf{q})|S_{l'\lambda',l\lambda}(\mathbf{q})|\chi_{\nu_i}(\mathbf{q})\rangle, \tag{2}$$

where $\mathbf{q}$ collectively represents the normal-mode coordinates and the index i denotes the vibrational mode. N_2O has three normal modes of vibration, namely, NO stretching, the doubly degenerate bending mode, and NN stretching, represented by ν_1, ν_2, and ν_3, respectively. The physical meaning of an element of the transformed scattering matrix is the scattering amplitude from one vibrational state, $\chi_{\nu_i}(\mathbf{q})$, of the target molecule to another, $\chi_{\nu_i'}(\mathbf{q})$. The vibrational frame transformation of Eq. (2) can only be performed if the fixed-nuclei S-matrix element, $S_{l'\lambda',l\lambda}$, is a smooth function of the incident electronic energy [36]. This means, in particular, that for this approach to be applicable, the fixed-nuclei S matrix should not have low-energy electronic resonances. As discussed above, the lowest electronic resonance in e^--NO_2 collisions occurs at collision energies of about 2.5 eV.

The cross section $\sigma_{\nu_i'\nu_i}$ for vibrational (de-)excitation can be obtained from the corresponding matrix element $S^{\nu_i'\nu_i}_{l'\lambda',l\lambda}$ by the expression

$$\sigma_{\nu_i'\nu_i}(E_{\rm el}) = \frac{\pi\hbar^2}{2m_eE_{\rm el}}\sum_{l'\lambda',l\lambda}\left|S^{\nu_i'\nu_i}_{l'\lambda',l\lambda} - \delta^{\nu_i'\nu_i}_{l'\lambda',l\lambda}\right|^2, \tag{3}$$

where m_e and $E_{\rm el}$ are, respectively, the reduced mass of the electron-N_2O system and the energy of the incident electron. Although the fixed-nuclei scattering matrix $S_{l'\lambda',l\lambda}(\mathbf{q})$ is weakly dependent on the energy, the remaining energy dependence introduces an ambiguity in the choice of the matrix in the integrand of Eq. (2). In the present calculation, we choose the following procedure: Integrating over the normal mode $\mathbf{q}$ in Eq. (2) for a given energy $E_{\rm el}$ of the electron in the incident channel (see the above equation) and at each integration point $\mathbf{q}$, the scattering matrix $S_{l'\lambda',l\lambda}(\mathbf{q})$ is taken from the R-matrix calculations performed at this particular fixed-nuclei geometry $\mathbf{q}$ and the electron scattering energy $E_{\rm el}$. Because the energy dependence of the fixed-nuclei scattering matrix is weak below 2.5 eV, the corresponding uncertainty of the final cross section is much smaller than the uncertainty related to the choice of the *ab initio* model (discussed below).

The cross section of Eq. (3) for vibrational excitation does not account for the rotational structure and can be compared with experiments or used in applications where the rotational structure of the initial and final vibrational levels is not important or not resolved. This is, generally, the case for most current experiments (including swarm measurements) and plasma applications at room or higher temperatures: With the rotational N_2O constant of $0.419\,01\ \mathrm{cm}^{-1} = 5.195\times10^{-5}$ eV [37] at 300 K, at least 25 rotational states are significantly populated.

Computational details

At its equilibrium geometry, N_2O has a linear asymmetric "N-N-O" molecular structure, described by the $C_{\infty v}$ symmetry point group with the group electronic state of the $^1\Sigma^+$ symmetry. The equilibrium geometry and the normal-mode coordinates with corresponding frequencies were computed

TABLE I. Energies $\hbar\omega_i$ (in eV) of N_2O normal modes obtained in the present study and compared with experimental data from Ref. [38].

			$\hbar\omega_i$	
Mode (ν_i)	Degeneracies	Symmetry	Experimental	Calculated
NO stretching (ν_1)	1	Σ^+	0.1610	0.1622
Bending (ν_2)	2	Π	0.0739	0.0761
NN stretching (ν_3)	1	Σ^+	0.2830	0.2849

with the MOLPRO suite [39] using the complete active space self-consistent field (CASSCF) method and the cc-pVTZ basis set [40] centered on each atom. N_2O has 22 electrons in a closed-shell electronic ground-state configuration given by

$$^1\Sigma^+ \colon 1\sigma^2 2\sigma^2 3\sigma^2 4\sigma^2 5\sigma^2 6\sigma^2 1\pi^4 7\sigma^2 2\pi^4.$$

In the calculations preserving the $C_{\infty v}$ symmetry group, the 10 electrons which occupy the lowest five σ molecular orbitals were kept frozen and the remaining 12 electrons were allowed to distribute themselves according to symmetry and spin restrictions in the complete active space (CAS) formed by the remaining $6\sigma 1\pi 7\sigma 2\pi$ ground-configuration orbitals and the next three molecular orbitals, 8σ, 9σ, and 3π, which are empty in the ground configuration. Because available quantum chemistry codes cannot handle continuous groups like $C_{\infty v}$, the calculations were performed in the C_{2v} group for the geometries describing NO and NN stretching displacements. For geometries breaking the $C_{\infty v}$ symmetry group—the bending-mode displacements—the same 10 electrons were kept frozen in the lowest 5 a' orbitals and the remaining 12 electrons were distributed in the 6–12 a' and 1–3 a'' orbitals of the corresponding C_s symmetry group.

Upon optimization of the equilibrium geometry, the N-N and N-O bond lengths were found to be 1.131 and 1.186 Å, respectively, in good agreement with the experimental values, 1.128 and 1.184 Å [38]. Table I reports a comparison between the obtained normal-mode frequencies and the available experimental data [38]. Our frequencies agree with the experimental references with a difference of less than 3%.

After characterizing the equilibrium geometry and normal-mode frequencies with MOLPRO [39], we carried out calculations of the potential energy of the ground electronic state of N_2O and calculations of continuum states using the U.K. *R*-matrix code [41] with the Quantemol-N suite [42]. For consistency with the MOLPRO calculations, we have used the same basis set and CAS. However, Quantemol-N does not have CASSCF built into it, and a series of convergence tests showed that the available complete active space configuration interaction (CAS-CI) model with the Hartree-Fock orbitals built with MOLPRO gave the best results. Figure 1 displays the ground-state electronic potential energy curves of N_2O for each normal mode obtained with Quantemol-N. For comparison, we also show the potential energy curves of harmonic oscillators generated with the frequencies obtained from MOLPRO. The Quantemol-N potential energy curves agree reasonably well with the potential energies calculated in the harmonic approximation. Small discrepancies are attributed to the anharmonicity of the actual N_2O potential. The permanent electric dipole moment of the target molecule obtained from the *R*-matrix calculation is 0.1 D, which is considered to be in satisfactory agreement with the experimental value, 0.16 D [38].

Using the molecular orbitals obtained from the structure calculations and the continuum Gaussian-type orbitals with partial waves up to $l \leqslant 4$, we performed the electronic continuum molecular states calculations with Quantemol-N. The radius of the *R*-matrix sphere was set to be 11 bohr. All the electronic states of the target below the cutoff energy, 16 eV, have been included in the close-coupling expansion. From the scattering calculations we can obtain the eigenphase sums and the reactance matrix (*K* matrix) at clumped nuclei.

Figure 2 displays the eigenphase sum of different irreducible representations at equilibrium and at displacements

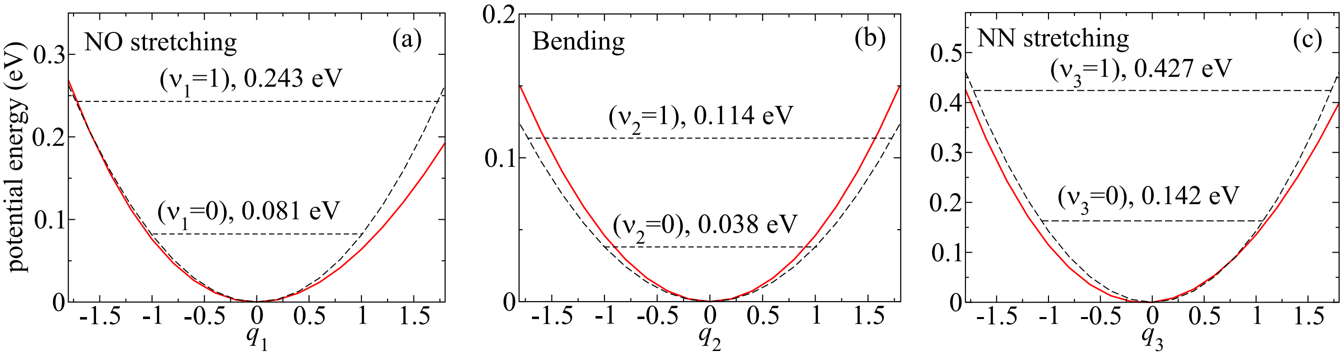

FIG. 1. Potential energy curves for the ground electronic state of N_2O as a function of the (a) NO stretching, (b) bending, and (c) NN stretching normal-mode coordinates. The abscissa axes represent dimensionless normal-mode coordinates. In each panel, only one mode is varied, while the other modes are kept fixed at their equilibrium positions. Solid red curves show the actual potential energies obtained from the *R*-matrix code, while dashed black curves represent energies calculated in the harmonic approximation, i.e., simply $\sim \frac{\hbar\omega_i}{2} q_i^2$. Dashed horizontal lines denote the energies of vibrational states.

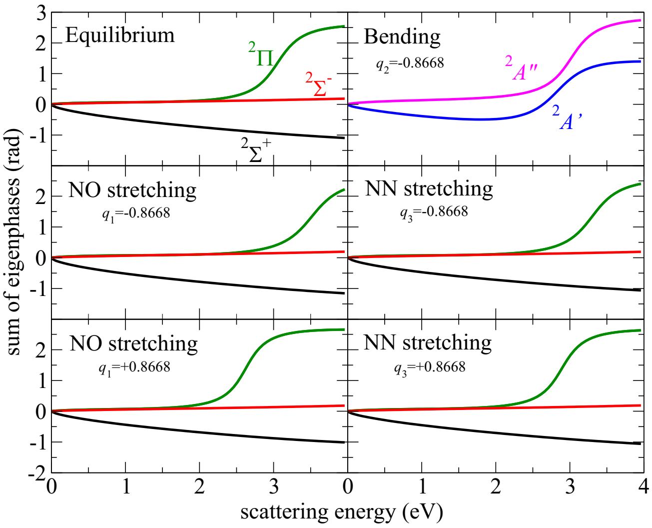

FIG. 2. Sum of eigenphases as a function of the electron scattering energy for equilibrium geometry and displacements $q_i = \pm 0.8668$ (dimensionless) along each normal mode. Due to the symmetry of the bending mode, the eigenphase sums of $q_2 = +0.8668$ and $q_2 = -0.8668$ are the same. The curves are color-coded according to the different symmetries of the $e^- + N_2O$ system.

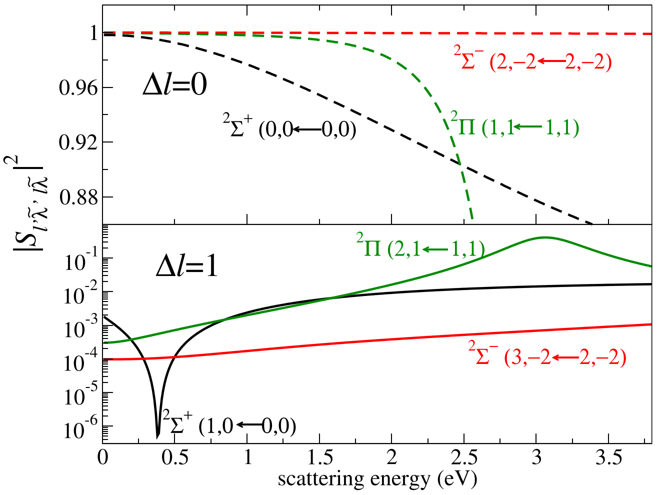

FIG. 3. Largest S-matrix elements (absolute values squared, $|S_{l'\tilde{\lambda}',l\tilde{\lambda}}|^2$) computed at the N_2O equilibrium geometry as a function of the scattering energy. Top: Couplings between channels with $\Delta l = 0$ in dashed curves. Bottom: Couplings between channels with $\Delta l = 1$ in solid curves.

away from the equilibrium along each normal-mode coordinate. We obtained the position and width of calculated resonances by fitting the eigenphase sum to a Breit-Wigner form. At equilibrium, the lowest resonance is found at 3.0 eV and has $^2\Pi$ symmetry. To compare with the available experimental data (the resonance around 2.3–2.5 eV [21,43]), the zero-point energy $\hbar(\omega_1 + 2\omega_2 + \omega_3)/2 = 0.3$ eV of the ground vibrational level should be accounted for. Therefore, in the present calculation, the energy of the resonance is 2.7 eV above the ground vibrational level. The difference from the experimental position of the resonance is attributed to the large uncertainty associated with the Born-Oppenheimer approximation used to identify the energy of the resonance in the theoretical calculation: The position of the resonance depends strongly on the choice of the fixed geometry near the N_2O equilibrium at which the scattering calculations were performed. In addition, the width (about 1 eV) of this shape resonance is larger than the difference between the experimental and the theoretical results.

The K matrix obtained from the scattering calculations was used to compute the clumped-nuclei scattering matrix (S matrix). Figure 3 displays selected dominant elements (the absolute value squared) of the S matrix at equilibrium geometry. In the figure (as well as in Fig. 4), the indices $\tilde{\lambda}$ refer to real-valued combinations of spherical harmonics $Y_l^{\pm\lambda}$ with positive and negative projections λ. The real-valued harmonics $Y_{l\tilde{\lambda}}$ with positive $\tilde{\lambda}$ transform as cosine-type functions with respect to the rotational angle ϕ about the axis z perpendicular to the plane of the molecule, while the harmonics with negative λ transform as sine-type functions. Except for the $S_{10,00}$ element, all other elements behave smoothly with the electronic energy below the first resonance. The minimum is observed near 0.4 eV for the 10 ← 00 transition.

Although the $S_{10,00}$ element has a strong energy dependence, which breaks the condition of the applicability of the vibrational frame transformation (the energy dependence should be smooth), its contribution to the VE cross section in Eq. (3) is negligible compared to that of the dominant terms (diagonal over $l\tilde{\lambda}$), and therefore, it does not compromise the present theoretical approach. The vibrationally transformed S matrix is calculated according to Eq. (2), where the integration over vibrational coordinates is performed numerically using a Gaussian-Legendre quadrature with 10 points.

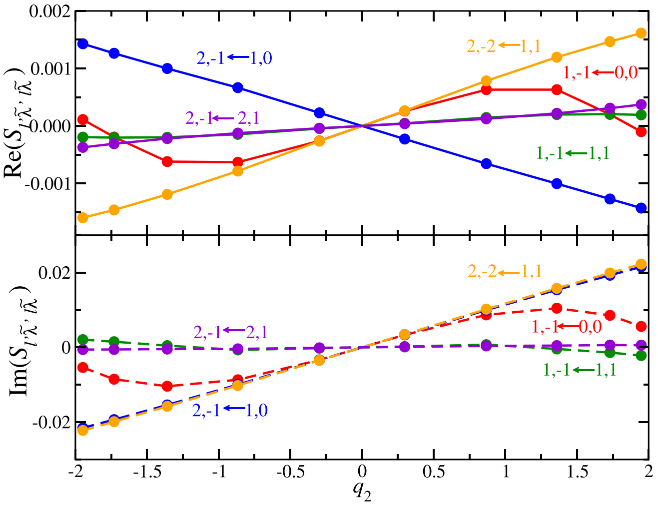

FIG. 4. Largest fixed-nuclei S-matrix elements as a function of the bending coordinate q_2, computed for scattering energy 0.26 eV. The upper (lower) panel shows the real (imaginary) part of the S-matrix elements. Couplings $l'\tilde{\lambda}' \leftarrow l\tilde{\lambda}$ between different partial waves, represented by real-valued harmonics $Y_{l,\tilde{\lambda}}$, are labeled by curves of different colors.

III. RENNER-TELLER COUPLING IN N_2O VIBRATIONAL EXCITATION BY ELECTRONS

It is instructive to analyze the dependence of major coupling elements of the scattering matrix as a function of the normal coordinates, especially for the bending mode. For the NO and NN stretching modes, the main contribution to the VE cross section is due to variation of the diagonal elements of the scattering matrix with low l.

In constrast, for the bending mode, the major contribution is due to the q_2 dependence of nondiagonal elements between the ${}^2\Sigma^+$ and the ${}^2\Pi$ states of the $e^- + N_2O$ system near the linear geometry. This is the Renner-Teller coupling, whose effect on electron-molecule collisions has been discussed in several previous studies [33,44–48]. For a linear triatomic (and larger) molecule with a ground electronic state of ${}^1\Sigma$ symmetry, the Renner-Teller effect couples σ and π partial waves of the incident electron with vibrational bending motion of the target molecule.

Due to the symmetry of the bending mode, all matrix elements $S_{l'\tilde{\lambda}',l\tilde{\lambda}}$ are symmetric or antisymmetric with respect to the change in the sign $q_2 \to -q_2$ of the displacement along the bending mode. The elements which are symmetric, such as diagonal and some nondiagonal elements, do not contribute to the vibrational excitation by one quantum of the bending mode. For an element $S_{l'\tilde{\lambda}',l\tilde{\lambda}}$ to be antisymmetric with respect to the $q_2 \to -q_2$ operation, one of $\tilde{\lambda}'$ and $\tilde{\lambda}$ should be negative, with the other positive or 0. In addition, there is a selection rule regarding the elements that do not vanish: For displacements along q_2, both spherical harmonics in $S_{l'\tilde{\lambda}',l\tilde{\lambda}}$ should be of a' or a'' irreducible representations of the C_s symmetry group (of the bent molecule). Figure 4 shows the largest (in magnitude) antisymmetric S-matrix elements as a function of the bending coordinate.

In Fig. 4, we see that most of the elements are linear with the q_2 coordinate, with the notable exception of $S_{1-1,00}$, which has a strong cubic dependence q_2^3. We attribute the significant cubic contribution to the coupling to the fact that the $s\sigma$ partial wave penetrates closer to the N_2O core electrons such that the linear approximation for the coupling between the $Y_{0,0}$ and the $Y_{1,-1}$ harmonics is no longer valid and higher terms are needed if a Taylor expansion is used to represent the coupling.

The linear dependence of the coupling between partial wave components in a linear molecule for small displacements along the bending coordinate is one of the main characteristics of the Renner-Teller effect. The effect cannot be easily observed in e^--N_2O scattering experiments, but it manifests itself in the bound states of the e^--N_2O system: Due to the degeneracy of the ${}^2\Pi$ electronic state of the e^--N_2O complex and the degenerate bending mode of N_2O, the relatively strong Renner-Teller coupling results in a bending configuration of the equilibrium geometry of the N_2O^- anion [49,50].

IV. CROSS SECTIONS AND RATE COEFFICIENTS

We calculated the vibrational (de-)excitation cross sections for transitions between the ground and the first excited vibrational states for each of the normal modes. Figure 5 displays a comparison of the theoretical $1 \leftarrow 0$ VE cross sections with the available experimental data [21,22,30], mentioned in Sec. I. None of the three experimental data resolve the $\nu_1 = 1/\nu_2 = 2$ and $\nu_3 = 1/\nu_1 = 2$ thresholds, i.e., the experimental cross section for the excitation of the NO mode ($\nu_1 = 0 \to 1$) includes also a contribution for the transition $\nu_2 = 0 \to 2$, and the cross section for the excitation of the NN mode includes a contribution for the $\nu_1 = 0 \to 2$ transition. But these additional contributions are expected to be significantly smaller due to the vibrational propensity rule: The transitions with a change of only one vibrational quantum are the largest. There is a significant disagreement between the experimental data, up to a factor of 20–50 for certain energies. On the other hand, the theoretical results also do not agree better with one or another experiment: For the NO stretching mode [Fig. 5(a)], the theory agrees better with the experiment by Hayashi [30]. For the bending mode [Fig. 5(b)], the theory agrees better with the other two experiments, although the agreement is quite poor. Note that the integral cross sections presented by Allan and Skalický [21] were obtained from the measured differential cross sections. Finally, for the NN stretching mode [Fig. 5(c)], the theory again agrees better with the data of Hayashi [30].

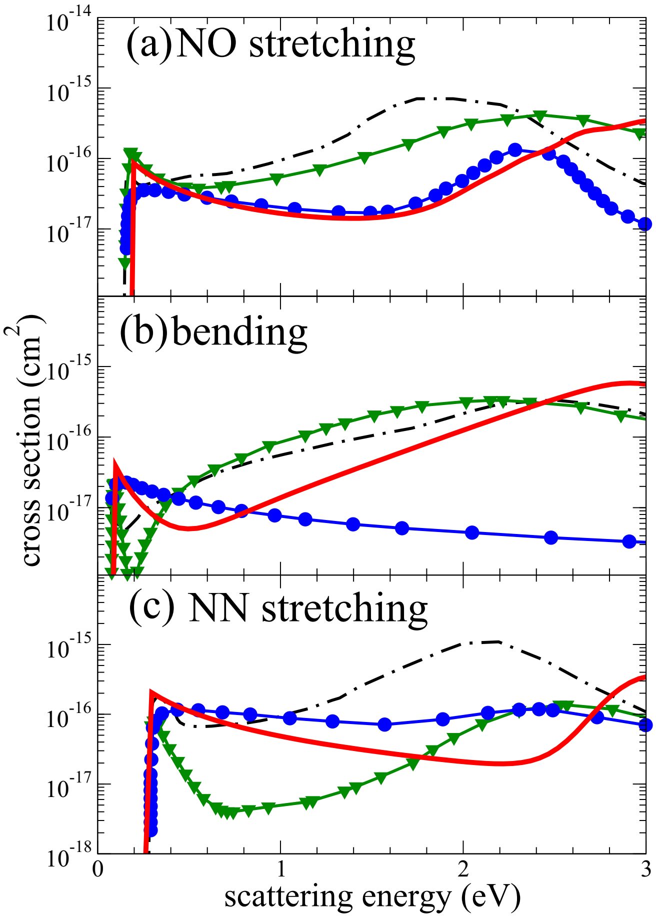

FIG. 5. Comparison of the present theoretical results with the available experimental cross sections for the vibrational $v = 0 \to v' = 1$ excitation of the (a) NO stretching, (b) bending, and (c) NN stretching modes. The experimental results are taken from Hayashi [30,31] (solid line with circles), Allan and Skalický [21] (solid line with triangles), and Nakamura [22] (dashed-dotted line).

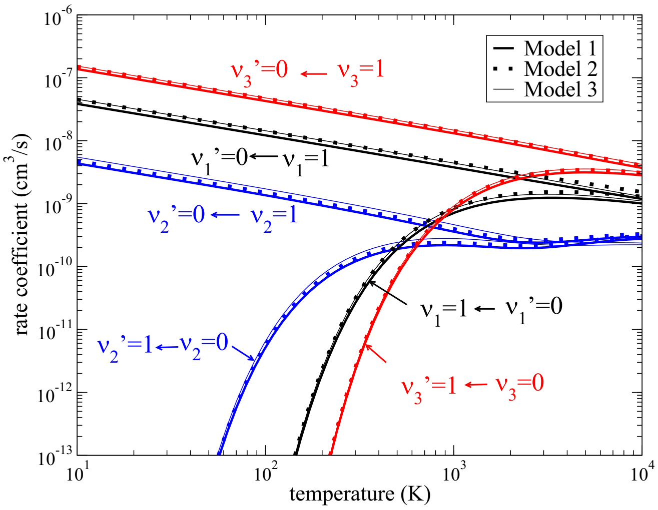

FIG. 6. Thermally averaged rate coefficients for excitation and de-excitation transitions between the ground and the first excited vibrational states of the NO stretching mode (black curves), bending mode (blue curves), and NN stretching mode (red curves). Vibrational (de-)excitations are labeled $\nu_i' \leftarrow \nu_i$. To provide an idea of the uncertainty of the present results, we also plotted the results of calculations with model 2 (dotted lines) and model 3 (thin lines). The three calculations produce curves that are almost indistinguishable.

In a recent review article [31], the swarm data of Nakamura [22], shown by the dashed-dotted lines in Fig. 5, were recommended as the most accurate among the available experimental cross sections. However, it should be stressed that the recommended swarm data may not be very accurate because of an ambiguity in their interpretation [22] (see the discussion in Secs. 3.3 and 3.5 in Ref. [31]). Therefore, the recommended experimental data should have a relatively large uncertainty and could be improved in a more accurate future experiment.

The present theoretical cross sections are expected to be valid only for energies below the energy of the $^2\Pi$ resonance mentioned above, i.e., below 2.3 eV. They are included in the Supplemental Material to this paper [51].

Thermally averaged rate coefficients $\alpha_{\nu_i'\nu_i}(T)$ for vibrational excitation are obtained from the cross sections of Eq. (3) using the standard formula

$$\alpha_{\nu_i'\nu_i}(T) = \frac{8\pi}{(2\pi k_B T)^{\frac{3}{2}}} \int_0^\infty \sigma_{\nu_i'\nu_i}(E_{\rm el}) e^{-\frac{E_{\rm el}}{k_B T}} E_{\rm el} dE_{\rm el}, \quad (4)$$

where k_B is the Boltzmann constant and T is the temperature. The computed rate coefficients are shown in Fig. 6 in different colors.

For convenient use in plasma models, the computed coefficients were also fitted using the analytical formula employed in our previous studies [36,52,53],

$$\alpha^{\rm fit}_{\nu_i'\nu_i}(T) = \frac{1}{\sqrt{T}} e^{-\frac{\Delta_{\nu_i'\nu_i}}{T}} P^{\rm fit}_{\nu_i'\nu_i}(x), \quad (5)$$

where $P^{\rm fit}_{\nu_i'\nu_i}(x)$ is a quadratic polynomial,

$$P^{\rm fit}_{\nu_i'\nu_i}(x) = a_0 + a_1 x + a_2 x^2 \quad \text{and} \quad x = \ln(T), \quad (6)$$

TABLE II. Parameters a_0, a_1, and a_2 of the polynomial $P^{\rm fit}_{\nu_i'\nu_i}(x)$ in Eqs. (5) and (6) for transitions between the ground and the first vibrational states in each normal mode. We specify the excitation threshold energies $\Delta_{\nu_i'\nu_i}$ of Eq. (7) in the second column. The threshold $\Delta_{\nu_i'\nu_i} = 0$ for the de-excitation process.

$1 \leftrightarrow 0$	$\Delta_{\nu_i'\nu_i}$ (K)	a_0	a_1	a_2
NO stretch	1888	1.22×10^{-7}	6.60×10^{-11}	-3.14×10^{-11}
Bending	885	1.37×10^{-8}	-2.50×10^{-11}	4.40×10^{-12}
NN stretch	3316	4.34×10^{-7}	7.42×10^{-10}	-5.20×10^{-10}

where $P^{\rm fit}_{\nu_i'\nu_i}(x) \approx P^{\rm fit}_{\nu_i'\nu_i}(x)$ can be viewed as the excitation and de-excitation probabilities, with $\Delta_{v'i',vi}$ being the threshold energy, defined as

$$\Delta_{\nu_i'\nu_i} = \begin{cases} E_{\nu_i'} - E_{\nu_i} > 0 & \text{for excitation,} \\ 0 & \text{for de-excitation.} \end{cases} \quad (7)$$

The numerically fitted parameters for vibrational excitation are listed in Table II. When the parameters listed in the table are used in the fitting formulas of Eqs. (5) and (6) with the temperature in kelvins, the obtained numerical values of the rate coefficients will be in units of cm^3/s.

V. UNCERTAINTY ESTIMATIONS

We have performed a number of calculations to assess the uncertainty of the obtained theoretical results. There are two main sources of uncertainty in the present theoretical approach. The first is the accuracy of the fixed-nuclei *S*-matrix elements computed for the polar molecule (with a small dipole moment) in the limited basis of spherical harmonics. It has been discussed by Liu [32]. The uncertainty associated with this approximation was estimated to be of the order of 6% for NO_2 [32]. It should not be larger for N_2O because it has a smaller dipole moment so that the couplings between partial waves induced by the permanent dipole moment of this molecule have a weaker effect on the final cross sections. Therefore, it is reasonable to assume that the corresponding uncertainty in the present case is below 6%.

The second source of uncertainty derives from the particular scattering model used in the calculation. The uncertainty can be assessed by performing a complete calculation with different parameters of the model. With the parameters discussed in Sec. II, referred to as model 1, we obtained the results shown above. In the second calculation, with model 2, the CAS in the configuration calculation was the same as in model 1 but a larger basis set, cc-pVQZ, was used. Finally, in the model 3 calculation the electronic basis set remained cc-pVTZ, but the CAS was reduced compared to that in model 1: 12 electrons were placed in frozen orbitals and the remaining 10 electrons in the lowest orbitals were allowed to be freely distributed in the active space. The rate coefficients obtained in the three models are shown in Fig. 6. The difference in the rate coefficients produced in the three models is about 6%. Consequently, the overall uncertainty of the present theoretical result is estimated to be below 12%.

VI. CONCLUSIONS

In this study, we computed cross sections for vibrational (de-)excitations of N_2O by a low-energy electron using (a) the normal-mode approximation to describe the vibrational states of the target molecule, (b) the R-matrix method to evaluate the fixed-nuclei electron-N_2O scattering matrices, and (c) the vibrational frame transformation to evaluate the amplitudes for vibrational transitions. In this approach, we neglected the rotational structure of each vibrational level, which corresponds to the situation where the rotational structure is not resolved in the initial and final states of the target molecule.

The computed results show a reasonable agreement with experimental data for the NO and NN stretching modes. For the bending mode the agreement is rather poor at energies above 0.4 eV. It was found that Renner-Teller coupling is responsible for the excitation of the bending mode, as was expected from general theoretical considerations. We are quite confident about the present theoretical cross sections for the bending mode because the numerical calculations of the fixed-nuclei scattering matrix fit well to the theory of Renner-Teller coupling. It should be stressed here that the most reliable experimental cross section for the bending mode by Nakamura [22,31] was obtained from swarm data and a direct measurement of the differential cross section at a single scattering angle by Allan and Skalický [21] and, therefore, may have a large uncertainty. This suggests that a better direct measurement of vibrational excitation in N_2O, at least for a few energies, is needed.

ACKNOWLEDGMENTS

This work was supported by the China Scholarship Council, the Thomas Jefferson Fund of the Office for Science and Technology of the Embassy of France in the United States, and National Science Foundation Grant No. PHY-1806915. It also received funding from the programs “Accueil des chercheurs étrangers” of CentraleSupélec and “Séjour à l’étranger 2019” of école doctorale INTERFACES of Université Paris-Saclay.

[1] L. M. Ziurys, A. Apponi, J. Hollis, and L. Snyder, Astrophys. J. **436**, L181 (1994).

[2] C. S. Jamieson, C. J. Bennett, A. M. Mebel, and R. I. Kaiser, Astrophys. J. **624**, 436 (2005).

[3] W.-C. Wang and N. D. Sze, Nature **286**, 589 (1980).

[4] N. Gherardi, S. Martin, and F. Massines, J. Phys. D: Appl. Phys. **33**, L104 (2000).

[5] Í. O’Sullivan and J. Benger, Emerg. Med. J. **20**, 214 (2003).

[6] A. Zecca, I. Lazzizzera, M. Krauss, and C. E. Kuyatt, J. Chem. Phys. **61**, 4560 (1974).

[7] R. I. Hall, A. Chutjian, and S. Trajmar, J. Phys. B: At. Mol. Opt. Phys. **6**, L365 (1974).

[8] E. Märk, T. D. Märk, Y. B. Kim, and K. Stephan, J. Chem. Phys. **75**, 4446 (1981).

[9] C. K. Kwan, Y. F. Hsieh, W. E. Kauppila, S. J. Smith, T. S. Stein, M. N. Uddin, and M. S. Dababneh, Phys. Rev. Lett. **52**, 1417 (1984).

[10] C. Szmytkowski, G. Karwasz, and K. Maciag, Chem. Phys. Lett. **107**, 481 (1984).

[11] L. Andric and R. Hall, J. Phys. B: At. Mol. Phys. **17**, 2713 (1984).

[12] D. Cubric, D. Cvejanovic, J. Jureta, S. Cvejanovic, P. Hammond, G. C. King, and F. H. Read, J. Phys. B: At. Mol. Phys. **19**, 4225 (1986).

[13] B. Marinkovic, C. Szmytkowski, V. Pejcev, D. Filipovic, and L. Vuskovic, J. Phys. B: At. Mol. Opt. Phys. **19**, 2365 (1986).

[14] W. M. Johnstone and W. R. Newell, J. Phys. B: At. Mol. Opt. Phys. **26**, 129 (1993).

[15] A. Zecca, J. C. Nogueira, G. P. Karwasz, and R. S. Brusa, J. Phys. B: At. Mol. Opt. Phys. **28**, 477 (1995).

[16] I. Iga, M. V. V. S. Rao, and S. K. Srivastava, J. Geophys. Res. E **101**, 9261 (1996).

[17] M. Kitajima, Y. Sakamoto, S. Watanabe, T. Suzuki, T. Ishikawa, H. Tanaka, and M. Kimura, Chem. Phys. Lett. **309**, 414 (1999).

[18] M. Kitajima, Y. Sakamoto, R. J. Gulley, M. Hoshino, J. C. Gibson, H. Tanaka, and S. J. Buckman, J. Phys. B: At. Mol. Opt. Phys. **33**, 1687 (2000).

[19] S. A. Rangwala, E. Krishnakumar, and S. V. K. Kumar, Phys. Rev. A **68**, 052710 (2003).

[20] A. Zecca, G. P. Karwasz, R. S. Brusa, and T. Wroblewski, Int. J. Mass Spectrom. **223-224**, 205 (2003).

[21] M. Allan and T. Skalický, J. Phys. B: At. Mol. Opt. Phys. **36**, 3397 (2003).

[22] Y. Nakamura, in *Proceedings of the 28th ICPIG*, edited by Institute of Plasma Physics AS CR (Czech Republic, Prague, 2007), pp. 224–226.

[23] H. Kawahara, D. Suzuki, H. Kato, M. Hoshino, H. Tanaka, O. Ingólfsson, L. Campbell, and M. J. Brunger, J. Chem. Phys. **131**, 114307 (2009).

[24] Y. Itikawa, At. Data Nucl. Data Tables **14**, 1 (1974).

[25] M. Kumar, Y. Kumar, N. Tiwari, and S. Tomar, J. At. Mol. Sci. **4**, 30 (2013).

[26] D. Nandi, V. S. Prabhudesai, and E. Krishnakumar, Phys. Chem. Chem. Phys. **16**, 3955 (2014).

[27] L. A. Morgan, C. J. Gillan, J. Tennyson, and X. Chen, J. Phys. B: At. Mol. Opt. Phys. **30**, 4087 (1997).

[28] B. K. Sarpal, K. Pfingst, B. M. Nestmann, and S. D. Peyerimhoff, J. Phys. B: At. Mol. Opt. Phys. **29**, 857 (1996).

[29] M. H. F. Bettega, C. Winstead, and V. McKoy, Phys. Rev. A **74**, 022711 (2006).

[30] M. Hayashi and K. Akashi, *Handbook of Plasma Material Science* (Ohm, Tokyo, 1992).

[31] M.-Y. Song, J.-S. Yoon, H. Cho, G. P. Karwasz, V. Kokoouline, Y. Nakamura, and J. Tennyson, J. Phys. Chem. Ref. Data **48**, 043104 (2019).

[32] H. Liu, S. F. dos Santos, C. H. Yuen, P. Cortona, V. Kokoouline, and M. Ayouz, Plasma Sources Sci. Technol. **28**, 105017 (2019).

[33] S. F. dos Santos, N. Douguet, V. Kokoouline, and A. Orel, J. Chem. Phys. **140**, 164308 (2014).

[34] V. Kokoouline, M. Ayouz, J. Z. Mezei, K. Hassouni, and I. F. Schneider, Plasma Sources Sci. Technol. **27**, 115007 (2018).

[35] E. Chang and U. Fano, Phys. Rev. A **6**, 173 (1972).

[36] X. Jiang, C. H. Yuen, P. Cortona, M. Ayouz, and V. Kokoouline, Phys. Rev. A **100**, 062711 (2019).

[37] G. Herzberg, *Electronic Spectra and Electronic Structure of Polyatomic Molecules*, Vol. 2 (Krieger, Malabar, FL, 1991).

[38] R. D. Johnson, *Computational Chemistry Comparison and Benchmark Database, NIST Standard Reference Database 101* (National Institute of Standards and Technology, Gaithersburg, Maryland, 2002), https://doi.org/10.18434/T47C7Z.

[39] H.-J. Werner, P. J. Knowles, G. Knizia, F. R. Manby, and M. Schütz, WIREs Comput. Mol. Sci. **2**, 242 (2012).

[40] R. A. Kendall, T. H. Dunning Jr., and R. J. Harrison, J. Chem. Phys. **96**, 6796 (1992).

[41] J. Tennyson, Phys. Rep. **491**, 29 (2010).

[42] J. Tennyson, D. B. Brown, J. J. Munro, I. Rozum, H. N. Varambhia, and N. Vinci, J. Phys.: Conf. Ser. **86**, 012001 (2007).

[43] A. Moradmand, A. L. Landers, and M. Fogle, Phys. Rev. A **88**, 012713 (2013).

[44] I. A. Mikhaylov, V. Kokoouline, A. Larson, S. Tonzani, and C. H. Greene, Phys. Rev. A **74**, 032707 (2006).

[45] N. Douguet, V. Kokoouline, and C. H. Greene, Phys. Rev. A **77**, 064703 (2008).

[46] N. Douguet, V. Kokoouline, and C. H. Greene, Phys. Rev. A **80**, 062712 (2009).

[47] N. Douguet, A. Orel, I. Mikhailov, I. F. Schneider, C. H. Greene, and V. Kokoouline, J. Phys.: Conf. Ser. **300**, 012015 (2011).

[48] N. Douguet, S. F. dos Santos, V. Kokoouline, and A. Orel, EPJ Web Conf. **84**, 07003 (2015).

[49] D. G. Hopper, A. C. Wahl, R. L. Wu, and T. O. Tiernan, J. Chem. Phys. **65**, 5474 (1976).

[50] G. S. Tschumper and H. F. Schaefer III, J. Chem. Phys. **107**, 2529 (1997).

[51] See Supplemental Material at http://link.aps.org/supplemental/10.1103/PhysRevA.102.032808 for the cross-section data.

[52] V. Kokoouline, A. Faure, J. Tennyson, and C. H. Greene, Mon. Not. R. Astron. Soc. **405**, 1195 (2010).

[53] M. Ayouz and V. Kokoouline, Atoms **4**, 30 (2016).